frontiers | Frontiers in Earth Science

TYPE Original Research
PUBLISHED 18 December 2024
DOI 10.3389/feart.2024.1511872

OPEN ACCESS

EDITED BY
Peng Wu,
Dalian University of Technology, China

REVIEWED BY
Zhengzheng Cao,
Henan Polytechnic University, China
Shuang Liang,
Northeast Petroleum University, China
Hun Lin,
Chongqing University of Science and Technology, China

*CORRESPONDENCE
Yuanyuan Li,
lyy08.syky@sinopec.com

RECEIVED 15 October 2024
ACCEPTED 19 November 2024
PUBLISHED 18 December 2024

CITATION
Li F, Li Y, Zhou T and Wang H (2024) Spontaneous imbibition characteristics and influencing factors of shale oil reservoir in Qintong depression.
Front. Earth Sci. 12:1511872.
doi: 10.3389/feart.2024.1511872

Spontaneous imbibition characteristics and influencing factors of shale oil reservoir in Qintong depression

Fengxia Li, Yuanyuan Li*, Tong Zhou and Haibo Wang

SINOPEC Petroleum Exploration and Production Research Institute, Beijing, China

This study integrates one-dimensional and two-dimensional nuclear magnetic resonance (NMR) techniques to conduct spontaneous imbibition experiments on two distinct lithologies (laminated calcareous shale and bulk clay-rich shale) from the Qintong Depression using four different fluid types. Field emission scanning electron microscopy (FE-SEM) and computed tomography (CT) scanning were employed to observe and track the dynamic changes in shale microstructures at specific intervals allowing for a comprehensive analysis of induced microfractures and their propagation patterns. These methods enabled a deeper understanding of the underlying mechanisms, enriching the interpretation of the imbibition results. The study reveals that anionic surfactants demonstrate exceptional performance during the imbibition process, and the combination of surfactants further enhanced oil recovery. The imbibition process can be divided into three stages: the imbibition diffusion stage, the transition stage, and the equilibrium stage, with the diffusion stage serving as the primary contributor, driven predominantly by capillary pressure. The calcareous shale cores exhibited the highest imbibition rates in the early stages, approaching equilibrium in the middle stages. Conversely, the clay-rich shale cores maintained relatively high imbibition rates throughout the second stage, indicating different imbibition dynamics based on lithology. NMR, CT scanning, and SEM analysis highlighted significant lithology-dependent differences in the mechanisms driving induced microfracture development during the imbibition and hydration. In laminated calcareous shale, imbibition and hydration primarily proceeded through the dissolution of calcareous minerals, resulting in pore expansion and induced microfractures along pre-existing fractures. In contrast, clay-rich shale exhibited similar mineral dissolution but also experienced clay swelling due to its high clay content, leading to the formation of bedding-parallel fractures with distinct directional patterns along weak mineral-matrix bonds. The experimental results underscored the pivotal role of lithology in determining final imbibition efficiency, with high-clay-content shales demonstrating superior recovery rates under spontaneous imbibition conditions. This study provides critical experimental data and insights into the microscopic mechanisms governing spontaneous imbibition across varied lithologies and fluid types in the Qintong Depression. The results offer foundational knowledge for optimizing oilfield development strategies.

KEYWORDS

imbibition, surfactant, hydration, pore structure, microfracture

1 Introduction

Shale oil, following shale gas, has emerged as another crucial unconventional energy resource, playing a significant role in the global energy alternative strategy (Fu and He, 2024). In 2022, a significant breakthrough in shale oil exploration and development was achieved in the Qintong Sag of China, with estimated shale oil resources in the Jiangsu exploration area reaching 12.7 $\times$ 10^8 t. Among these, the second member of the Paleogene Funing Formation (Funing 2 Member) in the Qintong Sag holds approximately 7.5 $\times$ 10^8 tonnes of resources. Currently, shale oil wells in this block have demonstrated promising production levels, with Well HY1 and Well H2C producing 29.7 t/day and 50.5 t/day of industrial oil flow, respectively, highlighting substantial development potential (Duan et al., 2024). To optimize the efficient development of shale oil from the Funing 2 Member, it is essential to enhance the parameters of the imbibition-enhancement process to boost the well productivity. The application of NMR technology to simulate and assess the microscopic mobilization of crude oil offers valuable insights for optimizing the field implementation of imbibition-enhanced recovery.

Traditional methods for assessing imbibition efficiency, such as volumetric and gravimetric techniques, face significant limitations when applied to shale oil reservoirs. These reservoirs are often characterized by tight formations, narrow pore throats, and challenges in establishing displacement pressure differentials, which complicate the experimental process (Guo et al., 2020). As a result, conventional techniques are prone to inaccuracies, typically providing only recovery data over time and exhibiting substantial experimental errors. Recent advancements in low-field NMR and CT scanning technologies have improved the study of the imbibition process by enabling the dynamic tracking of oil-water displacement and fluid saturation, offering greater precision and insights into pore-scale imbibition behavior (Liu and Sheng, 2019; Yan et al., 2024). Numerous researchers have conducted targeted studies on shale imbibition based on porous media imbibition theory, employing low-field NMR technology and core experiments to analyze the spontaneous imbibition dynamics in various shale blocks (Ge et al., 2015; Guo et al., 2020). Studies utilizing these technologies have identified capillary pressure and clay osmotic pressure as the primary drivers of shale imbibition, with imbibition capacity being strongly influenced by the content, type, and structure of clay minerals. Shale samples with higher clay content demonstrate greater cation exchange capacity and enhanced water absorption ability (Meng et al., 2020). Additionally, imbibition recovery is closely linked to the permeability, porosity, and natural fracture development of the rock samples (Ge et al., 2015; Guo et al., 2020). However, much of the existing research has predominantly focused on characterizing imbibition phenomena, with relatively few studies investigating the role of imbibition agents in enhancing recovery. Moreover, even fewer studies have been dedicated to optimizing the parameters of imbibition-enhancement processes, so there remains a lack of comprehensive and systematic evaluation methods for optimizing imbibition-enhanced recovery in shale oil reservoirs. Furthermore, while many researchers have conducted extensive studies on shale imbibition and hydration, these studies tend to be isolated, with limited integration of both aspects (Ding et al., 2022).

In summary, the specific characteristics of the factors influencing surfactant-assisted imbibition in shale reservoirs remain inadequately understood, and the mobilization of crude oil within the diverse micro-pore sizes during the imbibition process requires further investigation. Therefore, this study aims to bridge these gaps by characterizing the physical properties and pore size distribution of the shale reservoirs from the Funing 2 Member of the Qintong Depression and conducting spontaneous imbibition experiments using different surfactants. Through analysis of nuclear magnetic resonance (NMR) T_2 spectra, 2D spectra, variations in imbibition efficiency, and crude oil mobilization within the pores, this study seeks to clarify the effects of various factors on imbibition efficiency during surfactant-assisted imbibition in shale reservoirs. Additionally, the study explores the coupled effects of imbibition and hydration by closely monitoring dynamic changes in the shale's microstructure using field emission scanning electron microscopy (FE-SEM) and CT scanning. The propagation of induced microfractures and the underlying microscopic mechanisms are examined, providing an in-depth interpretation of the experimental results at the micro-scale. These findings aim to offer valuable insights into optimizing recovery efficiency in shale reservoirs, with a focus on surfactant-assisted imbibition processes.

2 Samples and methods

2.1 Liquids and core samples properties

For the preparation of the imbibition solution, four different surfactant systems were employed in the experiment: a 0.2% KCl system, an SDS system (0.2% KCl with an anionic surfactant), a SY system (0.2% KCl with a combination of anionic and non-ionic surfactants), and an HD system (0.2% KCl with a combination of anionic, non-ionic, and amphoteric surfactants) (Table 1).

The Funing 2 Member of Qintong Depression consists of deep lake and semi-deep lake shale characterized by strong vertical heterogeneity. Various types of reservoir spaces are developed within the shale, including tectonic fractures, bedding fractures and micro-pores, with porosity generally ranging from 3% to 6.29%. Specifically, cores were extracted from 1–42/49 of SD 201 well and 4–12/24 of HY 201 well. The core from SD 201 is bulk clay-rich shale, and the core from HY 201 well is laminated calcareous shale.

Mineral composition based on X-ray diffraction (XRD) testing was performed using a Rigaku D/MAX-2500pc X-ray diffractometer. Powder samples, ground to a fineness of 200–300 mesh, were placed on slides and gently pressed with a

TABLE 1 Type of surfactant in imbibition system.

Imbibition system	Type of surfactant
KCl	0.2% KCl
Single agent-SDS	Anion surfactant
Mixed agent-SY	Anionic surfactant + Non-ionic surfactant
Mixed agent-HD	Anionic surfactant + Nonionic surfactant + Amphoteric surfactant

TABLE 2 Physical properties of core and changes before and after experiment.

Sample no	Length (cm)	Diameter (cm)	Porosity (%)	Imbibition agent	Pore volume (cm^3)	Dry weight (g)	Wet weight (g)	Imbibition weight (g)
SD-1	5.037	2.511	5.19	0.2%KCL	1.294	62.7434	65.1438	65.0156
SD-2	5.081	2.513	7.05	0.5%SDS	1.776	61.3018	64.5963	64.3748
SD-3	5.045	2.517	6.51	0.5%HD	1.633	61.8529	64.8821	64.6535
SD-6	5.002	2.525	6.48	0.5%SY	1.622	61.2937	64.3025	64.0455
HY-2	5.064	2.451	2.04	0.2%KCL	0.487	62.9887	63.8921	63.8576
HY-3	5.072	2.535	1.35	0.5%SDS	0.345	63.2807	63.9207	63.8932
HY-4	5.042	2.533	1.26	0.5%HD	0.32	63.4344	64.028	63.9951
HY-6	5.067	2.528	2.13	0.5%SY	0.541	63.9349	64.9385	64.8835

glass slide to compact and fill the sample holder. The measurements were carried out with a tube voltage of 40 kV and a current of 40 mA, utilizing a Cu target and Ka-ray radiation. Diffraction data were collected at a scan rate of 4°/min, covering a scanning angle range of 4°–50°, with a step interval of 0.02°. Data processing for qualitative and quantitative mineral analysis was conducted using Jade 6.5 software.

The porosity of core samples measured in this study was measured using the helium porosity method. Due to the low molecular weight of helium, this method allows for more accurate measurement of small pore spaces, providing a closer estimate of the true porosity of the rocks. The helium porosity and air permeability of 8 core samples from the study area were determined using a PoroPDP-200 core pressure pore and permeability meter. Each core sample was approximately 5 cm in length and 2.5 cm in diameter. The experimental results are shown in Table 2.

2.2 Imbibition experiments

Before the imbibition experiment, shale samples were thoroughly washed and dried. The cores were cleaned using an extraction method in which the samples were placed in an extractor, and an oil-cleaning agent, a mixture of toluene and ethanol, was circulated via the siphon and steam pipe at the top and bottom of the extractor. The original fluid in the core was washed out until the oil-cleaning agent becomes clear. The cores were then saturated with crude oil using a vacuum saturation method.

In terms of NMR principles, when shale is saturated with a hydrogen-containing fluid, the NMR measures the relaxation signals of the fluid, rather than those of the shale matrix. The NMR T_2 relaxation time for fluid in larger pores is longer compared to fluid in smaller pores, meaning the relaxation time increases with pore size. Additionally, the amplitude of the relaxation signal corresponds to the volume of fluid in the pore, with a large amount of fluid corresponding to a higher signal amplitude. Therefore, NMR T_2 spectra can be utilized to quantitatively evaluate both the pore radius distribution and the fluid accumulation within pores during the spontaneous imbibition process in shale. The specific experimental steps are as follows: 1. The core sample was dried in an incubator at 105°C, until its mass remained constant. The T_1- T_2 spectrum and T_2 spectrum of the dry core were then measured using an NMR instrument; 2. The core was vacuum-saturated with crude oil. Field crude oil was placed in a pressurized tank, and the core was saturated under a pressure of 30 MPa for 10 days to ensure full saturation. The saturated core was then immersed in crude oil, and the T_1- T_2 and T_2 spectra were measured after saturation.3. Remove the saturated core with tweezers, surface oil was wiped off with gauze, and the core was placed into a beaker to begin the single-end spontaneous imbibition experiment; 4. At specified imbibition time (10 min, 30 min, 1 h, 1 day, 4 days, 8 days), the core was removed, the surface liquid was wiped off, the core's mass was measured, and the T_1- T_2 and T_2 spectra were recorded. This process was repeated until the T_2 signal no longer showed significant changes.

2.3 Microscopic experiments to interpret imbibition results

The NanoVoxel-2702E CT scanner was employed to scan different cross-sections before and after the spontaneous imbibition of core plugs at the same depth. The X-ray source provided a maximum power of 10 W and had a voltage limit of 150 kV. The scanner was equipped with three magnification lenses (×4, ×10, and ×20), offering a maximum theoretical resolution of 0.5 μm and a field of view of 25 cm. The charge coupled device (CCD) had a maximum resolution of 2048*2048 pixel. The object platform was capable of rotating from −180° to +180°. The hydration experiment was conducted as follows: (1) Core samples were dried in an oven for 48 h and then scanned by CT in their dry state; (2) The samples were placed in a beaker filled with water for hydration periods of 24 h, 72 h and 120 h; (3) After hydration, the samples were re-dried and subsequently scanned by CT.

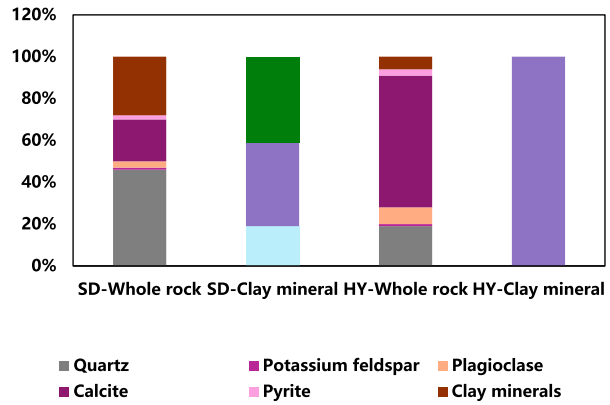

FIGURE 1
Mineral composition of the core used in the experiment.

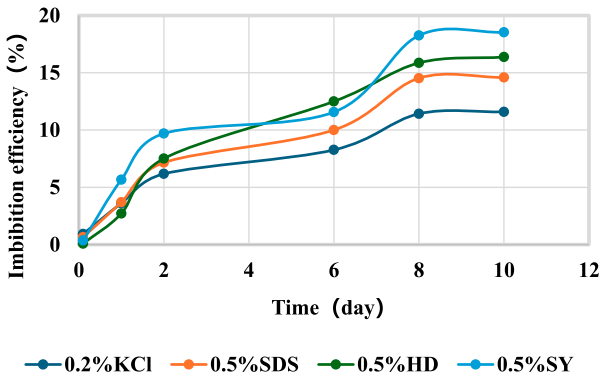

FIGURE 2
Summary of imbibition efficiency of SD bulk clay-rich shale for 1 h, 1 day, 2 days, 6 days, 8 days and 10 days under the action of 0.2% KCl, SDS, HD and SY surfactant.

For the FESEM analysis, a regular block sample with a dimension of 1.5 cm × 1.5 cm × 1 cm was selected for the experiment. The sample surface was first roughened with sandpaper and polishing liquid, and then polished with a Gatan 685C argon-ion polisher. After polishing, the samples were gold-coated and examined using a Hitachi Regulus8230 high-resolution scanning electron microscope (FESEM). The FESEM experiment has the following specifications: a maximum resolution of 0.8 nm; an acceleration voltage range of 0.01 kV–30 kV; magnification from ×20 to ×1,000,000, and a scanning speed of 80 s/frame to 25 s/frame. The experimental procedure involved immersing the sample in deionized water for various durations (1, 3, 5 days) to simulate hydration. Before electron microscope observation, the samples were dried to a constant weight under vacuum conditions to prevent water vapor from contaminating the electron microscope sample chamber. The dried samples were then analyzed again using FESEM to assess the changes in mineral composition, microfractures, and micropore structures of the shale before and after hydration.

3 Results

The XRD analysis results reveal that the primary minerals in the SD bulk clay-rich shale are quartz (46%), potassium feldspar (1%), plagioclase (3%), calcite (20%), pyrite (2%), and clay minerals (28%) (Figure 1). The dominant clay minerals in this sample include illite/smectite interstratified layers, illite, and chlorite. In contrast, the main mineral composition of the HY laminated calcareous shale core is primarily composed of quartz (19%), potassium feldspar (1%), plagioclase (8%), calcite (63%), pyrite (3%), and clay minerals (6%), with a lower clay content primarily composed of illite (Figure 1).

The porosity of the SD bulk clay-rich shale used in the imbibition experiment ranges from 5.19% to 7.05%, whereas the porosity of the HY shale core is significantly lower, ranging from 1.26% to 2.13%. Table 2 presents the different types of imbibition agents applied to each core, along with the corresponding changes in mass before and after imbibition.

3.1 Imbibition characteristics of SD bulk clay-rich shale

The T_2 spectra of the SD bulk clay-rich shale, measured at different imbibition times after oil saturation, reveal that the water phase signal gradually increases throughout the imbibition process and stabilizes around 8–10 days (Supplementary Figure S1). The pores primarily involved in imbibition replacement are small pores (<1 ms) and mesopores (1 ms–10 ms). The imbibition efficiency is calculated by dividing the difference between the T_2 spectral peak area at each time point and the initial peak area by the total T_2 area of the pore space. As shown in Figure 2, the imbibition process can be divided into three stages: in the early imbibition stage (<2 days), rapid imbibition replacement occurs preferentially in the connected pore throat near the core surface, resulting in a substantial volume of crude oil being produced. In the middle imbibition stage, as the imbibition liquid penetrates deeper into the pores, deep oil phase is replaced, leading to a slower increase in imbibition efficiency. In the later stage of imbibition, the imbibition efficiency remains nearly unchanged, indicating that imbibition has reached equilibrium by approximately 8 days. Among the different imbibition agents, the SY mixed agent demonstrated the highest efficiency, followed by the HD mixed agent, SDS, and finally the 0.2% KCl solution.

The interpretation of NMR results, particularly data from two-dimensional T_1-T_2 spectra, provides comprehensive insights into the saturation levels of different fluids within shale samples (Li et al., 2019; Li et al., 2020). Developed a fluid identification method using trapezoidal regions within the two-dimensional NMR T_1-T_2 spectrum (Supplementary Figure S3). By analyzing signals from different regions of the spectrum and correlating them with multi-step pyrolysis data, they created a fluid identification chart, which is particularly applicable to various types of organic-rich rocks. Unlike curve-shaped charts, the fixed boundaries of the trapezoidal regions provide greater consistency, making this approach a more reliable and universal T_1-T_2 chart for studying fluid properties in shale. In this study, the two-dimensional NMR T_1-T_2 spectrum was employed to investigate and analyze fluid occurrences in different lithologies of the Funing 2 Member. The established T_1-T_2 fluid identification spectrum (Figure 3) reveals that the original SD bulk

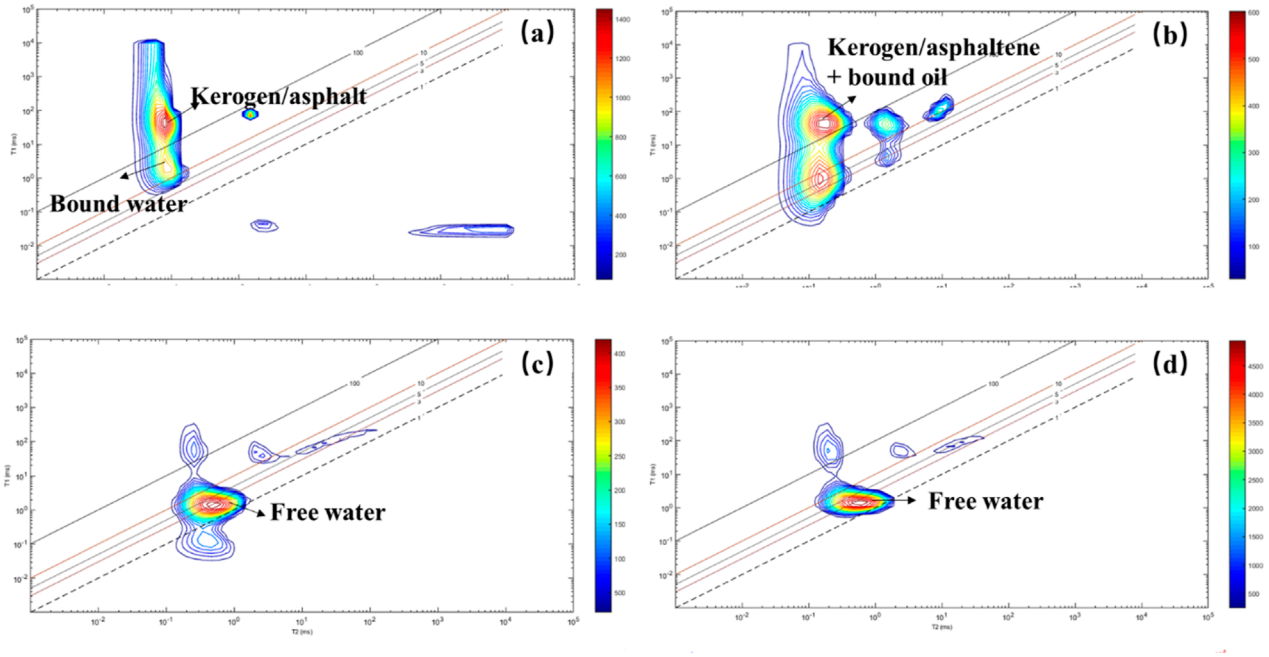

FIGURE 3
Changes of NMR 2D spectrum of SD bulk clay-rich shale under the action of 0.5% surfactant solution at different imbibition times. **(A)** Original sample; **(B)** Oil-saturated sample; **(C)** Imbibition for 48 h; **(D)** Imbibition for 120 h.

clay-rich shale samples show signals associated with residual kerogen/bitumen and clay mineral-bound water (Figure 3A). After oil saturation, signals of adsorbed oil are observed in the samples (Figure 3B). As the imbibition process progresses, the signals for organic matter and free oil decrease, while the signal intensity for free water increases (Figures 3C, D).

3.2 Microfracture propagation induced by SD clay-rich shale hydration

By comparing the macroscopic micro-fracture distribution characteristics of shale samples before and after water phase imbibition (Figure 4), it is evident that hydration significantly enhances the connectivity between pores and fractures within the rocks. Before hydration, the shale sample exhibited only one prominent microfracture. At the initial stage of hydration, the existing fractures first propagate along the parallel bedding planes, forming several distinct foliation fractures. As hydration progresses, both the width and length of these parallel fractures expand substantially, and some fractures connected to form a new fracture network. This development further increases both the fracture volume and surface area, thereby enhancing fluid transport pathway within the shale.

Based on an understanding of the macroscopic microfracture development characteristics, this study further employs dynamic observation techniques combined with energy spectrum analysis to perform fixed-point monitoring and elemental testing at specific microstructural locations. The objective is to analyze the dynamic expansion patterns of induced microfractures and identify key controlling factors. Using multi-point *in-situ* scanning technology, changes in the microstructure of shale samples before and after hydration were tracked and compared. Initially, SEM was used to examine the micro-pore structure of the samples prior to hydration, with characteristic points marked and natural fractures characterized. After various imbibition periods, the samples were positioned macroscopically and observed *in situ*. Continuous imaging at different magnifications was conducted at the same locations to identify and analyze correlations between mineral composition and micro-pore structures (Figure 5). SEM observations revealed a distinct dissolution of rhombohedral carbonate minerals within the shale matrix during the first 24 h of hydration (Figures 5A, B, E, F, I, J), with most dissolution occurring within this period, and minor changes in pore size afterward (Figures 5B–D, J–L). Additionally, the evolution of original natural fractures during hydration was clearly observed. The fracture evolution trends observed through *in-situ* SEM were closely aligned with the water saturation changes detected by NMR and the fracture volume changes observed through CT scanning. Microfractures on the original shale surface initially developed into hydration fractures within the first day, after which they stopped widening and even gradually closed between days 3 and 5, demonstrating an initial widening followed by closure. This behavior is likely associated with the swelling of clay minerals, which affects their water absorption capacity. Furthermore, on the third day of hydration, oil droplets were observed accumulating around larger pores and microfractures under SEM (Figures 5G, K). By the fifth day, oil-water displacement became clearly visible, with oil droplets effectively expelled from the shale matrix (Figures 5H, L). These observations suggest that, during the imbibition process, the migration and aggregation of the oil phase are significantly influenced by the evolving pore structure and microfracture network.

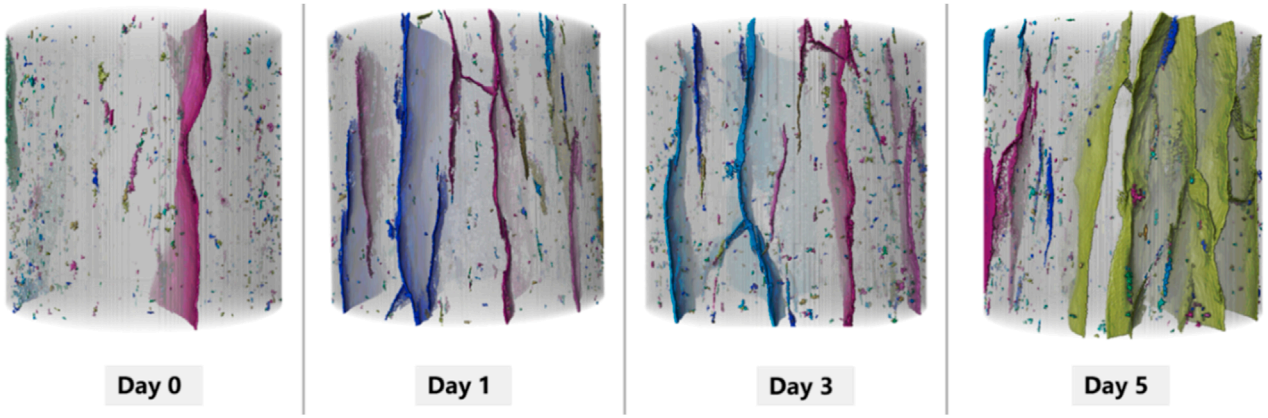

FIGURE 4
3D reconstruction of fractures based on CT scanning before and after imbibition of SD bulk clay-rich shale.

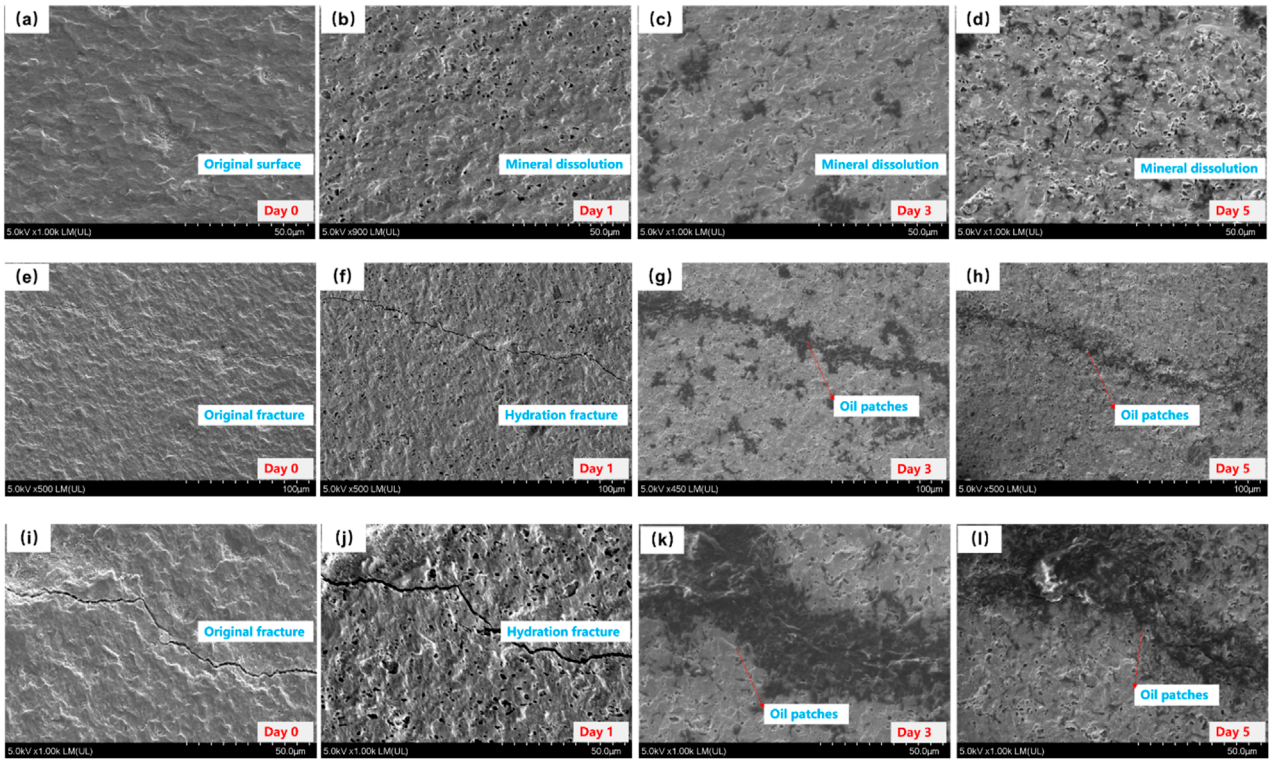

FIGURE 5
Scanning electron microscopy (SEM) observation of the imbibition process of the SD clay-rich shale shows the changes of pore structure during the imbibition process **(A–D)**, and the evolution of the original natural fracture development area **(E–L)**.

3.3 Imbibition characteristics of HY laminated calcareous shale

The evolution of the T_2 spectra at various stages of imbibition for the oil-saturated core of the HY laminated calcareous shale reveals that the water-phase signal gradually increases during the imbibition process, stabilizing after approximately 8–10 days (Supplementary Figure S2). The pore intervals primarily involved in the displacement are micropores (<1 ms) and mesopores (1 ms–10 ms). The imbibition efficiency can be quantified by dividing the difference between the T_2 peak area and the initial peak area by the total pore T_2 area. As illustrated in Figure 6, the core's imbibition process can be divided into three stages: 1. Early stage (<1.5 days): Rapid imbibition displacement occurs in the connected pore throats near the core surface, driven by capillary forces, resulting in the quick expulsion of a significant

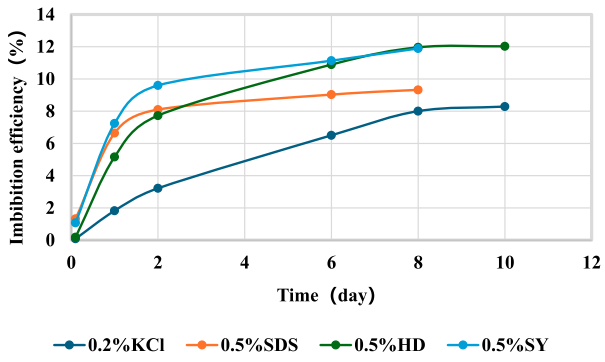

FIGURE 6
Summary of imbibition efficiency of HY laminated calcareous shale for 1 h, 1 day, 2 days, 6 days, 8 days and 10 days under the action of 0.2%KCl, SDS, HD and SY surfactant.

amount of oil. 2. Middle stage: The imbibition liquid infiltrates deeper pores, displacing oil from these deeper regions, but the rate of increase in imbibition efficiency slows down. 3. Late stage: Imbibition efficiency plateaus, with little to no change, achieving equilibrium after 6–8 days. In terms of imbibition performance, the SY surfactant and HD surfactant demonstrate the best results, followed by the single surfactant agent, while 0.2% KCl exhibits the least effect.

According to the established T_1-T_2 fluid identification map (Figure 7), the original core of the HY laminated calcareous shale primarily exhibits signals corresponding to clay mineral-bound water and weakly bound oil (Figure 7A). After oil saturation, signals corresponding to adsorbed oil become prominent (Figure 7B). As the imbibition process progresses, the signals from organic matter and free oil gradually diminish, while the intensity of the free water signal steadily increases (Figures 7C, D).

3.4 Microfracture propagation induced by HY laminated calcareous shale hydration

CT scanning results of HY laminated calcareous shale core samples (Figure 8) reveal significant development of microfractures during water infiltration. Hydration leads to the widening and extension of pre-existing fractures. In areas with dense pore networks, smaller cracks merge to form new, larger fractures. During the early stage of hydration, fractures predominantly form parallel to the bedding. However, as hydration progresses, intersection between the original fractures, which are perpendicular to the bedding, begin to emerge, thereby enhancing fracture connectivity. Additionally, beyond hydration-induced fractures, 3D reconstructions reveal the formation of larger pores, likely due to mineral dissolution. This dissolution process weakens the original cementation and facilitates the growth of the interconnected fracture network.

Building on the understanding of macroscopic microfracture development, fixed-point dynamic observation combined with energy spectrum testing was employed to analyze the expansion patterns of induced microfractures and identify key controlling factors. The original surface morphology of the HY laminated calcareous shale (Figure 9A) and the changes observed 1, 3, and 5 days after hydration reveal extensive dissolution of rhombohedral carbonate minerals (Figures 9B–D). This continuous dissolution facilitates the formation of microfractures, which progressively expand into larger and intersecting cracks (Figure 9D). Additionally, the accumulation of oil droplets in shaded regions illustrates the process of oil-water displacement during hydration, where oil in smaller pores is displaced into larger pores and expelled through newly formed microfractures (Figures 9B–D). Mineral dissolution also occurs along the boundaries of more stable minerals that are less susceptible to hydration, such as quartz and albite (Figures 9E, F), leading to the shedding and migration of larger mineral particles. Fractures preferentially form and propagate along boundaries with significant differences in mineral composition, especially around pyrite (Figures 9G, H). As hydration continues, the original fractures further expand (Figures 9I, J). Elemental surface scanning reveals that the fracture areas are primarily composed of carbonate minerals, while silicate minerals are more prevalent on the sides. Fracture expansion is primarily driven by the dissolution of carbonate minerals (Figures 9K, L).

4 Discussion

Imbibition recovery is influenced by numerous factors, which can generally be categorized into two groups: those related to the intrinsic properties of the reservoir, such as reservoir type, porosity and permeability, boundary conditions, and reservoir fluid properties; and those related to the properties of the injected fluids used for imbibition-enhanced oil recovery (Hu et al., 2020; Li et al., 2021; Shaibu and Guo, 2021; Yang et al., 2023).

4.1 Comparison of imbibition efficiency of different surfactant

This study highlights the superior performance of surfactant mixtures, particularly the combination of anionic, non-ionic, and amphoteric surfactants, in enhancing imbibition efficiency, when compared to pure anionic surfactants or water alone. Oil displacement surfactants can be classified into four main categories based on their ionization behavior and the nature of their functional groups: non-ionic, amphoteric, cationic, and anionic surfactants (Ge et al., 2015; Meng et al., 2017; Pal et al., 2018; Das et al., 2019; Massarweh and Abushaikha, 2020; Bashir et al., 2022; Isaac et al., 2022). These surfactants exhibit distinct characteristics that influence their ability to alter the wettability of reservoir rocks under varying conditions. Anionic surfactants, which ionize in aqueous solutions to carry a negative charge, are widely used in various products (Wu et al., 2017). In chemical enhanced oil recovery, they are commonly employed in sandstone reservoirs due to their low adsorption rates and good thermal stability (Kamal et al., 2017). High molecular weight anionic surfactants, particularly sulfonate, sulfate, and carboxylate types, are effective at reducing interfacial tension (IFT) to ultra-low levels and can maintain stability across a wide range of pH conditions (Yang et al., 2010). Non-ionic surfactants possess a polar head group with

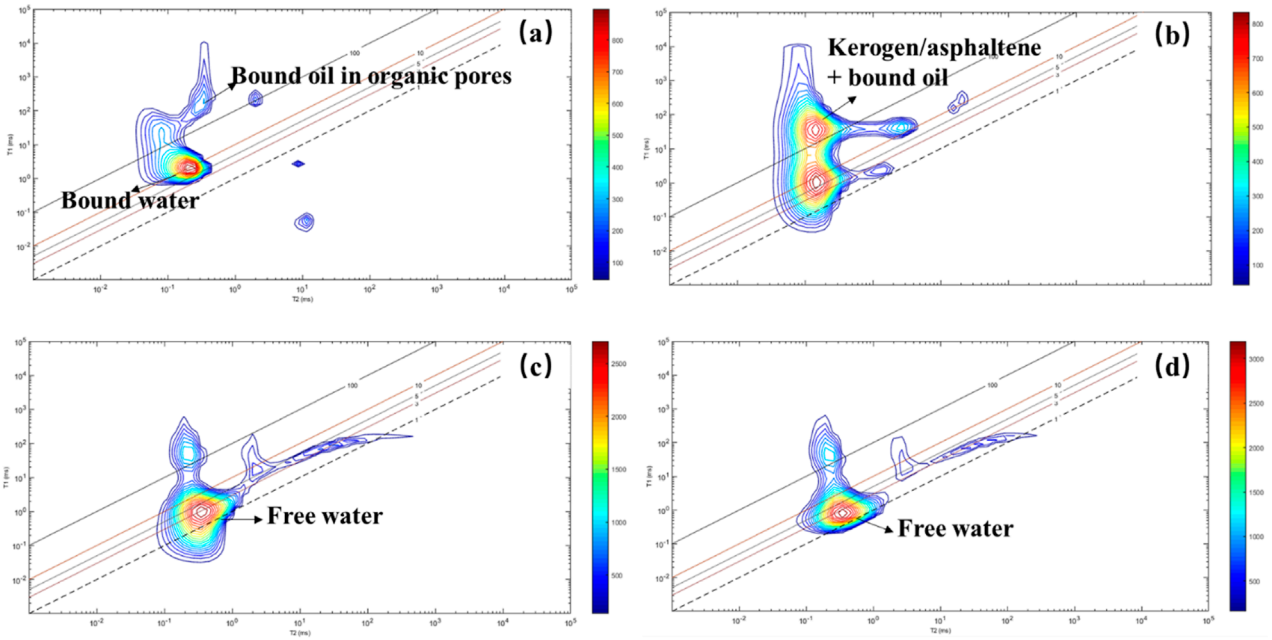

FIGURE 7
Changes of 2D NMR spectra of HY laminated calcareous shale under the action of 0.5% surfactant solution at different imbibition times. **(A)** Original sample; **(B)** Oil-saturated sample; **(C)** Imbibition for 48 h; **(D)** Imbibition for 120 h.

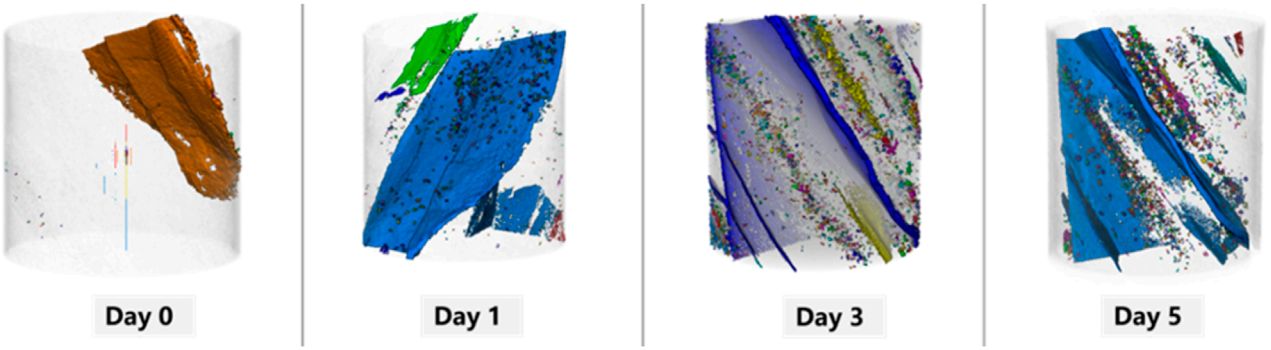

FIGURE 8
3D fracture reconstruction of HY laminated calcareous shale cores based on CT scanning before and after imbibition.

a strong affinity for water, but they do not ionize in solution. These surfactants are primarily influenced by hydrogen bonding and van der Waals interactions (Kamal et al., 2017). As the temperature increases, the strength of hydrogen bonding weakens, leading to reduced solubility of the surfactant in the aqueous phase (Zhao et al., 2005). Non-ionic surfactants generally exhibit a lower ability to reduce interfacial tension (IFT) compared to their ionic counterparts (Iglauer et al., 2009). Amphoteric surfactants can carry either a positive or negative charge depending on the solution's pH (Lv et al., 2011). These surfactants have shown promising potential for enhanced oil recovery applications, especially under high-temperature and high-salinity conditions (Kamal et al., 2017; Massarweh and Abushaikha, 2020). The inclusion of amphoteric surfactants in surfactant mixtures provides additional stability and improves the fluid's performance in complex reservoir environments (Lv et al., 2011).

The suitability of different surfactants for various types of reservoirs stems from their distinct mechanisms for altering wettability (Karambeigi et al., 2016; Jing et al., 2019; Liu and Sheng, 2019; Liu et al., 2019). In comparison to conventional surfactant systems, the mixture of anionic, non-ionic, and amphoteric surfactants in this study demonstrated superior performance in shale oil imbibition recovery. This improvement can be attributed to the synergistic effects of these surfactants in enhancing wettability, reducing IFT, and improving emulsification properties. Anionic surfactants are highly effective in altering rock wettability by desorbing organic matter and reducing interfacial tension (IFT) between oil and water, facilitating better oil recovery.

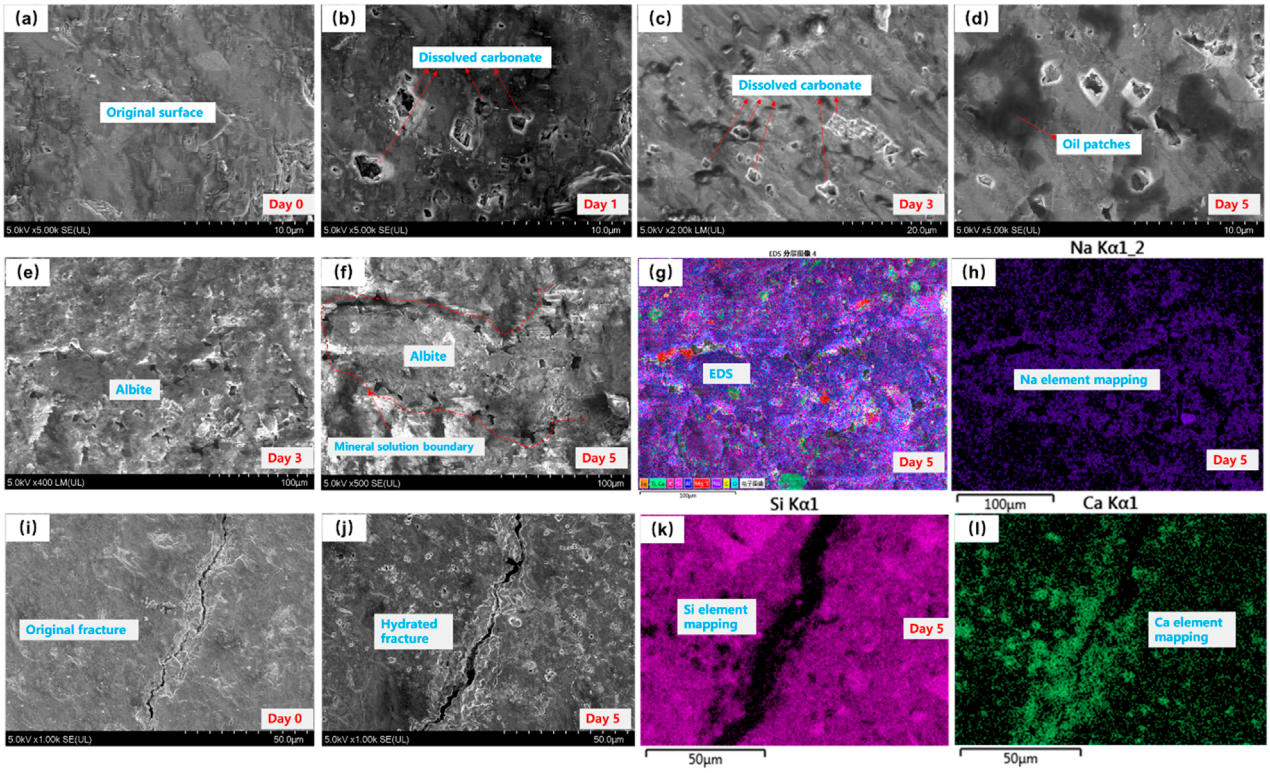

FIGURE 9
Laminated calcareous shale hydration process based on SEM observation. **(A)** The original substrate surface; **(B–D)** Substrate surface after 1 day, 3 days, 5 days of hydration; **(E, F)** The dissolution boundary of albite minerals after 3 days, 5 days of hydration; **(G)** A layered image of Figure **(F)**; **(H)** Distribution of Na elements of Figure **(F)**; **(I)** Original surface micro-cracks; **(J)** The initial crack widens after hydration; **(K, L)** Distribution of Si and Ca elements in fracture and matrix area of Figure **(J)**.

Non-ionic surfactants, on the other hand, interact with rock surfaces through hydrophobic interactions, further enhancing wettability and reducing IFT, albeit to a lesser degree than anionic surfactants. Amphoteric surfactants provide additional stability and adaptability under challenging reservoir conditions, such as high salinity and temperature. When combined, these surfactants complement each other's strengths, enhancing overall performance by improving wettability, reducing IFT, stabilizing emulsions, and increasing the effectiveness of oil displacement in complex reservoir environments. The synergistic interactions between the surfactants in a mixed system not only optimize the individual benefits of each surfactant but also contribute to more efficient oil recovery, making mixed surfactant formulations a highly effective strategy for improving imbibition efficiency in shale oil reservoirs.

This result is consistent with previous studies that supports the effectiveness of mixed surfactant systems in enhancing oil recovery in complex reservoirs such as shale (Lv et al., 2011; Alvarez and Schechter, 2017; Das et al., 2019; Qin et al., 2019; Habibi et al., 2020; Kesarwani et al., 2021; Xiao et al., 2021; Yahya et al., 2022). The results of this study emphasize the potential of mixed surfactant formulations to improve imbibition efficiency, offering valuable insights for the optimization of enhanced oil recovery methods in shale reservoirs under challenging conditions.

4.2 Comparison of imbibition efficiency of shales with different lithologies

Apart from the type of imbibition agent, this study reveals that the imbibition efficiency in shale reservoirs is closely linked to their lithology, with clay mineral content playing a particularly pivotal role in the hydration process. Specifically, the imbibition efficiency of SD clay-rich shale was found to be higher than that of HY laminated calcareous shale. This difference in performance is not solely due to variations in initial porosity, but rather to the higher clay content in SD shale, which enhances imbibition through osmotic pressure and the formation of additional hydration-induced fractures. In contrast, the imbibition process in HY laminated calcareous shale, which has a lower clay content, primarily relies on the dissolution of carbonate minerals.

The high clay content in SD shale significantly influences its imbibition characteristics. Clay minerals, which are abundant in shale reservoirs, act as non-ideal semi-permeable membranes. These minerals create a chemical potential difference, allowing specific ions to pass through and driving water molecules into the nanopores of the clay (You et al., 2019; Hu et al., 2020; Liu et al., 2022; Yang et al., 2023). In high-salinity environments, clay minerals generate excess negative charges due to lattice substitution. To maintain electrical neutrality, water molecules and cations adsorb onto the mineral surface, forming a double electric layer

(Dominijanni and Manassero, 2012; Røyne et al., 2015; Fritz et al., 2020). When exposed to low-salinity water, osmotic pressure induces water molecules to enter the clay pores, leading to cation desorption and increased repulsion within the double electric layer (Wilson and Wilson, 2014; Du et al., 2018). This osmotic process not only promotes the expansion of the clay but also generates pore pressure, which further pushes crude oil out, enhancing imbibition.

In contrast, the lower clay content in HY laminated calcareous shale leads to a less pronounced osmotic effect. Instead, imbibition in this lithology primarily occurs due to the dissolution of carbonate minerals. The high levels of pyrite and carbonate minerals in HY laminated calcareous shale make pyrite oxidation a key trigger for these dissolution processes (Ali and Hascakir, 2017). When exposed to water and oxygen, pyrite oxidizes, creating an acidic environment, which accelerates the dissolution of carbonate minerals like calcite, which unstable under acidic conditions (Zhuang et al., 2024). This process alters the mineral composition and promotes the expansion of primary fractures and formation of secondary cracks during hydration (Du et al., 2018). Electron microscopy observations further confirm these lithological differences, highlighting the significant impact of mineral composition on the hydration process. In conclusion, the differences in imbibition efficiency between the SD clay-rich shale and HY laminated calcareous shale can be attributed to the variations in their mineral composition and the mechanisms driving the imbibition process, with osmotic pressure and mineral dissolution playing distinct roles in each lithology.

5 Conclusion

This study systematically investigates the effects of surfactant combinations on shale imbibition recovery, demonstrating that these combinations significantly enhance recovery rates and play a critical role in optimizing imbibition efficiency. The imbibition process was divided into three stages: the imbibition diffusion stage, the imbibition transition stage, and the imbibition equilibrium stage. Among these, the diffusion stage proved the most effective, with capillary pressure being the main driving force in the initial phase. The HY laminated calcareous shale core exhibited the highest imbibition rate during the early stage and reached equilibrium in the middle stage. In contrast, the SD clay-rich shale core maintained a high imbibition rate in the transition stage.

Advanced analytical techniques, including NMR, CT, and SEM analyses revealed significant differences in the mechanisms of microfracture development during water infiltration, depending on lithological characteristics. In laminated calcareous shale, water infiltration primarily led to pore expansion and the formation of induced microfractures through the dissolution of calcareous minerals, which also expanded pre-existing fractures. In contrast, massive clay shale experienced a similar dissolution process, but with the additional effect of clay expansion, resulting in distinct bedding fractures. These fractures demonstrated clear directionality, preferentially expanding along the weak bonding surfaces between minerals and the rock matrix.

The findings highlight the crucial role of lithology in determining the final imbibition effect. Shales with higher clay content exhibited improved recovery under spontaneous imbibition conditions. This study provides a foundational theoretical framework and practical guidance for optimizing shale oil and gas recovery, illustrating that a detailed understanding of lithological variations can lead to more efficient resource development strategies. This study demonstrates that surfactant combinations significantly enhance imbibition recovery rates, offering a practical approach to improve shale oil and gas extraction efficiency. The findings underscore the importance of tailoring surfactant types and concentrations to specific lithological characteristics, suggesting potential for optimized recovery in varied shale reservoirs. Future research should focus on investigating the long-term effects under field conditions and evaluating the impact of temperature, pressure, and other external factors on the imbibition process for broader application.

Data availability statement

The raw data supporting the conclusions of this article will be made available by the authors, without undue reservation.

Author contributions

FL: Conceptualization, Supervision, Writing–review and editing. YL: Writing–original draft. TZ: Data curation, Investigation, Writing–review and editing. HW: Funding acquisition, Supervision, Writing–review and editing.

Funding

The author(s) declare that financial support was received for the research, authorship, and/or publication of this article. This work was supported by National Natural Science Foundation project (No. 52374066), Joint Funds of the National Natural Science Foundation of China (Grant No. U23B6004), Project from Science and Technology Department of Sinopec (P23190).

Conflict of interest

Authors FL, YL, TZ, and HW were employed by SINOPEC Petroleum Exploration and Production Research Institute.

The authors declare that this study received funding from Sinopec. The funder had the following involvement in the study: Funding acquisition, Supervision.

Generative AI statement

The author(s) declare that no Generative AI was used in the creation of this manuscript.

Publisher's note

All claims expressed in this article are solely those of the authors and do not necessarily represent those of

their affiliated organizations, or those of the publisher, the editors and the reviewers. Any product that may be evaluated in this article, or claim that may be made by its manufacturer, is not guaranteed or endorsed by the publisher.

Supplementary material

The Supplementary Material for this article can be found online at: https://www.frontiersin.org/articles/10.3389/feart.2024.1511872/full#supplementary-material

References

Ali, M., and Hascakir, B. (2017). Water/rock interaction for eagle ford, marcellus, green river, and barnett shale samples and implications for hydraulic-fracturing-fluid engineering. *SPE J.* 22, 162–171. doi:10.2118/177304-PA

Alvarez, J. O., and Schechter, D. S. (2017). Wettability alteration and spontaneous imbibition in unconventional liquid reservoirs by surfactant additives. *SPE Reserv. Eval. and Eng.* 20, 107–117. doi:10.2118/177057-PA

Bashir, A., Sharifi Haddad, A., and Rafati, R. (2022). A review of fluid displacement mechanisms in surfactant-based chemical enhanced oil recovery processes: analyses of key influencing factors. *Petroleum Sci.* 19, 1211–1235. doi:10.1016/j.petsci.2021.11.021

Das, S., Adeoye, J., Dhiman, I., Bilheux, H. Z., and Ellis, B. R. (2019). Imbibition of mixed-charge surfactant fluids in shale fractures. *Energy and Fuels* 33, 2839–2847. doi:10.1021/acs.energyfuels.8b03447

Ding, Y., Liu, X., Liang, L., Xiong, J., and Hou, L. (2022). Experimental and model analysis on shale spontaneous imbibition and its influence factors. *J. Nat. Gas Sci. Eng.* 99, 104462. doi:10.1016/j.jngse.2022.104462

Dominijanni, A., and Manassero, M. (2012). Modelling the swelling and osmotic properties of clay soils. Part II: the physical approach. *Int. J. Eng. Sci.* 51, 51–73. doi:10.1016/j.ijengsci.2011.11.001

Du, J., Hu, L., Meegoda, J. N., and Zhang, G. (2018). Shale softening: observations, phenomenological behavior, and mechanisms. *Appl. Clay Sci.* 161, 290–300. doi:10.1016/j.clay.2018.04.033

Duan, H., Wen, Z., Qiu, Y., Teng, J., He, T., and Liu, S. (2024). Organic petrography and geochemistry of the fu 2 member of the paleocene Funing Formation, gaoyou depression, subei basin, eastern China: implications for shale oil potential. *Unconv. Resour.* 4, 100066. doi:10.1016/j.uncres.2023.100066

Fritz, C. J., Asce, A. M., Shackelford, C. D., and Malusis, M. A. (2020). Determining maximum chemico-osmotic pressure difference across clay membranes. *J. Geotechnical Geoenvironmental Eng.* 146, 06019018. doi:10.1061/(asce)gt.1943-5606.0002196

Fu, E., and He, W. (2024). The development and utilization of shale oil and gas resources in China and economic analysis of energy security under the background of global energy crisis. *J. Petroleum Explor. Prod. Technol.* 14, 2315–2341. doi:10.1007/s13202-024-01818-3

Ge, H.-K., Yang, L., Shen, Y.-H., Ren, K., Meng, F.-B., Ji, W.-M., et al. (2015). Experimental investigation of shale imbibition capacity and the factors influencing loss of hydraulic fracturing fluids. *Petroleum Sci.* 12, 636–650. doi:10.1007/s12182-015-0049-2

Guo, J., Li, M., Chen, C., Tao, L., Liu, Z., and Zhou, D. (2020). Experimental investigation of spontaneous imbibition in tight sandstone reservoirs. *J. Petroleum Sci. Eng.* 193, 107395. doi:10.1016/j.petrol.2020.107395

Habibi, A., Esparza, Y., Boluk, Y., and Dehghanpour, H. (2020). Enhancing imbibition oil recovery from tight rocks by mixing nonionic surfactants. *Energy fuels.* 34, 12301–12313. doi:10.1021/acs.energyfuels.0c02160

Hu, Y., Zhao, C., Zhao, J., Wang, Q., Zhao, J., Gao, D., et al. (2020). Mechanisms of fracturing fluid spontaneous imbibition behavior in shale reservoir: a review. *J. Nat. Gas Sci. Eng.* 82, 103498. doi:10.1016/j.jngse.2020.103498

Iglauer, S., Wu, Y., Shuler, P., Tang, Y., and Goddard, W. A. (2009). Alkyl polyglycoside surfactant–alcohol cosolvent formulations for improved oil recovery. *Colloids Surfaces A Physicochem. Eng. Aspects* 339, 48–59. doi:10.1016/j.colsurfa.2009.01.015

Isaac, O. T., Pu, H., Oni, B. A., and Samson, F. A. (2022). Surfactants employed in conventional and unconventional reservoirs for enhanced oil recovery—a review. *Energy Rep.* 8, 2806–2830. doi:10.1016/j.egyr.2022.01.187

Jing, W., Huiqing, L., Genbao, Q., Yongcan, P., and Yang, G. (2019). Investigations on spontaneous imbibition and the influencing factors in tight oil reservoirs. *Fuel* 236, 755–768. doi:10.1016/j.fuel.2018.09.053

Kamal, M. S., Hussein, I. A., and Sultan, A. S. (2017). Review on surfactant flooding: phase behavior, retention, IFT, and field applications. *Energy and Fuels* 31, 7701–7720. doi:10.1021/acs.energyfuels.7b00353

Karambeigi, M. S., Nasiri, M., Haghighi Asl, A., and Emadi, M. A. (2016). Enhanced oil recovery in high temperature carbonates using microemulsions formulated with a new hydrophobic component. *J. Industrial Eng. Chem.* 39, 136–148. doi:10.1016/j.jiec.2016.05.020

Kesarwani, H., Saxena, A., Mandal, A., and Sharma, S. (2021). Anionic/Nonionic surfactant mixture for enhanced oil recovery through the investigation of adsorption, interfacial, rheological, and rock wetting characteristics. *Energy and Fuels* 35, 3065–3078. doi:10.1021/acs.energyfuels.0c03767

Li, G., Su, Y., Guo, Y., Hao, Y., and Li, L. (2021). Frontier enhanced oil recovery (EOR) research on the application of imbibition techniques in high-pressure forced soaking of hydraulically fractured shale oil reservoirs. *Geofluids* 2021, 1–17. doi:10.1155/2021/6634357

Li, J., Jiang, C., Wang, M., Lu, S., Chen, Z., Chen, G., et al. (2020). Adsorbed and free hydrocarbons in unconventional shale reservoir: a new insight from NMR T1-T2 maps. *Mar. Petroleum Geol.* 116, 104311. doi:10.1016/j.marpetgeo.2020.104311

Li, J., Lu, S., Chen, G., Wang, M., Tian, S., and Guo, Z. (2019). A new method for measuring shale porosity with low-field nuclear magnetic resonance considering non-fluid signals. *Mar. Petroleum Geol.* 102, 535–543. doi:10.1016/j.marpetgeo.2019.01.013

Liu, J., and Sheng, J. J. (2019). Experimental investigation of surfactant enhanced spontaneous imbibition in Chinese shale oil reservoirs using NMR tests. *J. Industrial Eng. Chem.* 72, 414–422. doi:10.1016/j.jiec.2018.12.044

Liu, J., Sheng, J. J., Wang, X., Ge, H., and Yao, E. (2019). Experimental study of wettability alteration and spontaneous imbibition in Chinese shale oil reservoirs using anionic and nonionic surfactants. *J. Petroleum Sci. Eng.* 175, 624–633. doi:10.1016/j.petrol.2019.01.003

Liu, K., Wang, D., Sheng, J. J., and Li, J. (2022). Review of the generation of fractures and change of permeability due to water-shale interaction in shales. *Geofluids* 2022, 1–20. doi:10.1155/2022/1748605

Lv, W., Bazin, B., Ma, D., Liu, Q., Han, D., and Wu, K. (2011). Static and dynamic adsorption of anionic and amphoteric surfactants with and without the presence of alkali. *J. Petroleum Sci. Eng.* 77, 209–218. doi:10.1016/j.petrol.2011.03.006

Massarweh, O., and Abushaikha, A. S. (2020). The use of surfactants in enhanced oil recovery: a review of recent advances. *Energy Rep.* 6, 3150–3178. doi:10.1016/j.egyr.2020.11.009

Meng, M., Ge, H., Shen, Y., Hu, Q., Li, L., Gao, Z., et al. (2020). The effect of clay-swelling induced cracks on imbibition behavior of marine shale reservoirs. *J. Nat. Gas Sci. Eng.* 83, 103525. doi:10.1016/j.jngse.2020.103525

Meng, Q., Liu, H., and Wang, J. (2017). A critical review on fundamental mechanisms of spontaneous imbibition and the impact of boundary condition, fluid viscosity and wettability. *Adv. Geo-Energy Res.* 1, 1–17. doi:10.26804/ager.2017.01.01

Pal, S., Mushtaq, M., Banat, F., and Al Sumaiti, A. M. (2018). Review of surfactant-assisted chemical enhanced oil recovery for carbonate reservoirs: challenges and future perspectives. *Petroleum Sci.* 15, 77–102. doi:10.1007/s12182-017-0198-6

Qin, T., Goual, L., and Piri, M. (2019). Synergistic effects of surfactant mixtures on the displacement of nonaqueous phase liquids in porous media. *Colloids Surfaces A Physicochem. Eng. Aspects* 582, 123885. doi:10.1016/j.colsurfa.2019.123885

Røyne, A., Dalby, K. N., and Hassenkam, T. (2015). Repulsive hydration forces between calcite surfaces and their effect on the brittle strength of calcite-bearing rocks. *Geophys. Res. Lett.* 42, 4786–4794. doi:10.1002/2015GL064365

Shaibu, R., and Guo, B. (2021). The dilemma of soaking a hydraulically fractured horizontal shale well prior to flowback – a decade literature review. *J. Nat. Gas Sci. Eng.* 94, 104084. doi:10.1016/j.jngse.2021.104084

Wilson, M. J., and Wilson, L. (2014). Clay mineralogy and shale instability: an alternative conceptual analysis. *Clay Miner.* 49, 127–145. doi:10.1180/claymin.2014.049.2.01

Wu, G., Yuan, C., Ji, X., Wang, H., Sun, S., and Hu, S. (2017). Effects of head type on the stability of gemini surfactant foam by molecular dynamics simulation. *Chem. Phys. Lett.* 682, 122–127. doi:10.1016/j.cplett.2017.06.017

Xiao, Z., Dexin, L., Yue, L., Lulu, L., and Jie, Y. (2021). Synergistic effects between anionic and amphoteric surfactants on promoting spontaneous imbibition in ultra-low permeability reservoirs: study of mechanism and formula construction. *Colloids Surfaces A Physicochem. Eng. Aspects* 625, 126930. doi:10.1016/j.colsurfa.2021.126930

Yahya, Z. N. M., Puspaseruni, N. P., Kurnia, R., Wahyuningrum, D., Mulyani, I., Wijayanto, T., et al. (2022). The effect of aluminosilicate in anionic–nonionic surfactant mixture on wetness and interfacial tension in its application for enhanced oil recovery. *Energy Rep.* 8, 1013–1025. doi:10.1016/j.egyr.2021.11.269

Yan, X., Dai, C., Wang, R., Liu, H., Meng, S., Jin, X., et al. (2024). Experimental study on countercurrent imbibition in tight oil reservoirs using nuclear magnetic resonance

and AFM: influence of liquid–liquid/solid interface characteristics. *Fuel* 358, 130026. doi:10.1016/j.fuel.2023.130026

Yang, H., Britton, C., Liyanage, P. J., Solairaj, S., Kim, D. H., Nguyen, Q., et al. (2010). "Low-cost, high-performance chemicals for enhanced oil recovery," in *SPE improved oil recovery symposium*. doi:10.2118/129978-MS

Yang, Y., Wang, S., Feng, Q., Cao, X., Qin, Y., Shu, C., et al. (2023). Imbibition mechanisms of fracturing fluid in shale oil formation: a review from the multiscale perspective. *Energy fuels.* 37, 9822–9840. doi:10.1021/acs.energyfuels.3c00502

You, L., Zhou, Y., Kang, Y., Yang, B., Cui, Z., and Cheng, Q. (2019). Fracturing fluid retention in shale gas reservoirs: mechanisms and functions. *Arab. J. Geosci.* 12, 779. doi:10.1007/s12517-019-4955-2

Zhao, G., Khin, C. C., Chen, S. B., and Chen, B.-H. (2005). Nonionic surfactant and temperature effects on the viscosity of hydrophobically modified hydroxyethyl cellulose solutions. *J. Phys. Chem. B* 109, 14198–14204. doi:10.1021/jp051955c

Zhuang, Y., Zhang, T., Liu, X., Zhang, S., Liang, L., and Xiong, J. (2024). Intrinsic mechanisms of shale hydration-induced structural changes. *J. Hydrology* 637, 131433. doi:10.1016/j.jhydrol.2024.131433